J Eng Math (2012) 75:15–27
DOI 10.1007/s10665-011-9504-2

A comparison study of the Boussinesq and the variable density models on buoyancy-driven flows

Hyun Geun Lee · Junseok Kim

Received: 23 March 2011 / Accepted: 23 August 2011 / Published online: 7 October 2011
© Springer Science+Business Media B.V. 2011

Abstract When density variations are sufficiently small the Boussinesq approximation is valid. The approximation is introduced to reduce the degree of the complexity of density variations and implies that density effects are considered only in the buoyancy force term of the momentum equation. Because of its simplicity in practical implementations, the approximation is widely used. Although there are many studies related to the approximation, some important characteristics are still missing. In this article, we compare the Boussinesq approximation and variable density models for the two-dimensional (2D) Rayleigh–Taylor instability with a phase-field method. Numerical experiments indicate that for an initially symmetric perturbation of the interface the symmetry of the heavy and light fronts for the Boussinesq model can be seen for a long time. However, for the variable density model, the symmetry is lost although the flow starts symmetrically.

Keywords Boussinesq approximation model · Phase-field method · Projection method · Rayleigh–Taylor instability · Variable density model

1 Introduction

In fluids, the dynamic variables typically required to describe the motion are the velocity, pressure, viscosity, and density. The density is a very important quantity for fluids since it determines fluid properties, such as compressibility. Because of the complexity of density variations in fluids, some assumptions have been introduced to reduce the degree of the complexity. One of these assumptions is the Boussinesq approximation [1], which is used in the field of buoyancy-driven flows.

Assume that the densities ρ_1 and ρ_2 (ρ_1 and ρ_2 are the densities of the heavier and lighter fluid, respectively) are uniform on each side of the interface, and that the density difference is small in the sense that the Atwood number $At = (\rho_1 - \rho_2)/(\rho_1 + \rho_2)$ is small. The Boussinesq approximation can be made in this case and is also related to the assumption that all of the accelerations of flow are small compared to the gravitational acceleration. In this approximation, the background density can be treated as a constant ρ_*, i.e., the variation of background

H. G. Lee · J. Kim (✉)
Department of Mathematics, Korea University, Seoul 136-701, Republic of Korea
e-mail: cfdkim@korea.ac.kr

density is neglected, and the difference between the actual density and ρ_* will contribute only to the buoyancy force term of the momentum equation [2]. Because of its simplicity in practical implementations (we solve a constant instead of a variable coefficient Poisson equation), the Boussinesq approximation is employed in many previous articles [3–16]. On the other hand, many numerical methods (e.g., front tracking [17–21], volume of fluid [22–26], lattice Boltzmann [27–30], level set [31–34], and phase-field [35–38] methods) have been proposed to study the Rayleigh–Taylor instability for the variable density model. However, there has been no comparison studies on the different models, to authors' knowledge.

In order to understand the difference of the basic dynamics between two different models, we focus on the Rayleigh–Taylor instability. The Rayleigh–Taylor instability is an instability of an interface between two fluids with different densities, which occurs when the lighter fluid is pushing the heavier fluid. And the instability is characterized by the Atwood number. The Rayleigh–Taylor instability for a fluid in a gravitational field was originally introduced by Rayleigh [39] and later applied to all accelerated fluids by Taylor [40]. This instability has been applied to a wide range of problems, such as inertial confinement fusion [41], supernova explosion [42], nuclear weapon explosion [43], oceanography [44], atmospheric physics [45], and supernova remnant [46]. In this article, we employ a phase-field model to study the two-dimensional (2D) Rayleigh–Taylor instability. This method replaces sharp fluid interfaces by thin but nonzero thickness transition regions where the interfacial forces are smoothly distributed [47]. The basic idea is to introduce a conserved order parameter ϕ that varies continuously over thin interfacial layers and is mostly uniform in the bulk phases. The advantages of this approach are topology changes without difficulties; interfaces can either merge [48] or break up [49] and no extra coding is required; the concentration field ϕ has physical meanings not only on the interface but also in the bulk phases; it can be naturally extended to multicomponent systems [50] and three space dimensions [51] with a straightforward manner.

The article is organized as follows. The governing equations are introduced in Sect. 2. In Sect. 3, we briefly review previous studies using the Boussinesq approximation. We discuss the Boussinesq approximation of the incompressible Navier–Stokes equations in Sect. 4. Numerical results are presented in Sect. 5. In Sect. 6, conclusions are drawn. In the Appendix A, we derive the discrete scheme and numerical solution. We also present the approximate projection method used to solve the discrete Navier–Stokes equations.

2 Governing equations

The equations governing the motion of unsteady, viscous, incompressible, immiscible two-fluid system are the Navier–Stokes equations (the subscript i denotes the ith fluid component):

$$\rho_i \left(\frac{\partial \mathbf{u}_i}{\partial t} + \mathbf{u}_i \cdot \nabla \mathbf{u}_i \right) = -\nabla p_i + \nabla \cdot [\eta_i (\nabla \mathbf{u}_i + \nabla \mathbf{u}_i^T)] + \rho_i \mathbf{g} \quad \text{in } \Omega_i,$$
$$\nabla \cdot \mathbf{u}_i = 0 \quad \text{in } \Omega_i,$$

where ρ_i is the density, $\mathbf{u}_i$ is the velocity, p_i is the pressure, and η_i is the viscosity of fluid $i = 1, 2$, the superscript T denotes the transpose, and $\mathbf{g}$ is the gravitational force. A schematic of a two-phase domain is shown in Fig. 1.

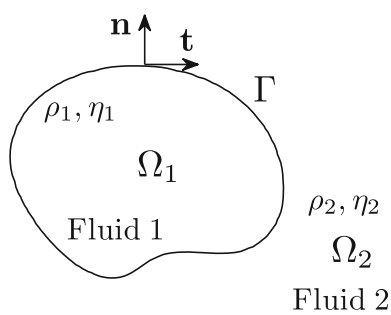

Fig. 1 Schematic of a two-phase domain

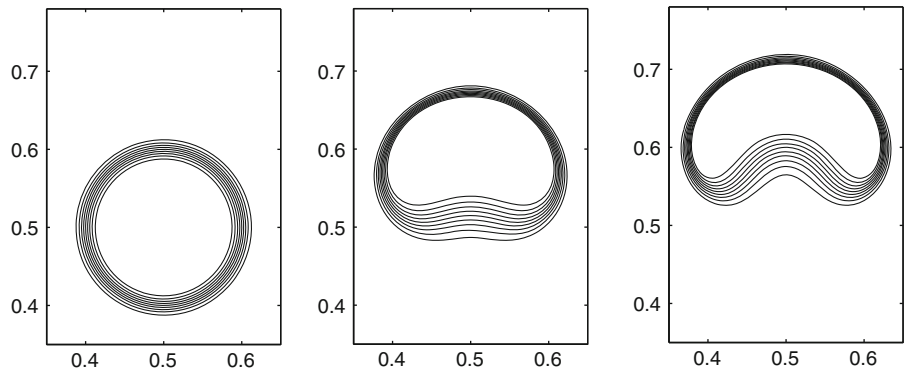

(a) $t = 0$ **(b)** $t = 0.72$ **(c)** $t = 0.96$

Fig. 2 Contour plots of time evolution of the density field. The times are shown below each figure

Γ is the interface between two fluids, $\mathbf{n} = (n_1, n_2)$ is the outward unit normal vector to the interface, and $\mathbf{t} = (t_1, t_2)$ is the unit tangent vector to the interface.

In fluid flow problems with moving interfaces, part of the interface of the computational domain is unknown and must be determined as part of the solution. On the unknown interface, the boundary conditions should be satisfied. The dynamic condition requires that the forces acting on the fluid at the interface be in equilibrium (momentum conservation at the interface). This means that the normal forces on either side of the interface are of equal magnitude and opposite direction, while the forces in the tangential direction are of equal magnitude and direction [52] (neglecting surface tension):

$$(\mathbf{n} \cdot \tau)_1 \cdot \mathbf{n} = -(\mathbf{n} \cdot \tau)_2 \cdot \mathbf{n} \quad \text{and} \quad (\mathbf{n} \cdot \tau)_1 \cdot \mathbf{t} = (\mathbf{n} \cdot \tau)_2 \cdot \mathbf{t},$$

where τ is the stress tensor (including pressure terms). The kinematic condition requires that the interface be a sharp boundary separating the two fluids that allows no flow through it. This states that the components of the velocity normal (or tangential) to the interface are equal for two fluids:

$$\mathbf{u}_1 \cdot \mathbf{n} = \mathbf{u}_2 \cdot \mathbf{n} \quad \text{and} \quad \mathbf{u}_1 \cdot \mathbf{t} = \mathbf{u}_2 \cdot \mathbf{t}.$$

The density field is passively convected by the fluid velocity:

$$\rho_t + \nabla \cdot (\rho \mathbf{u}) = 0.$$

However, using this form of the transport equation may cause significant problems in computation of two-fluid flows. We will give an example about how this form causes problems. Consider a light bubble rising under gravity in a heavy background fluid. The initial conditions are a zero velocity field and a density field:

$$\rho(x, y, 0) = \frac{\rho_1 + \rho_2}{2} + \tanh\left(\frac{100(\sqrt{(x-0.5)^2 + (y-0.5)^2} - 0.1)}{\sqrt{2}}\right)$$

on the unit square domain. Here, $\rho_1 = 1$ and $\rho_2 = 3$ (ρ_1 and ρ_2 are densities inside and outside the bubble, respectively). The viscosity is matched and is given as $\eta = 0.1$. Contour plots of time evolution of the density field from the calculation with a mesh size 256×256 are shown in Fig. 2. These show the rise of the bubble. However, there is unphysical numerical compression and diffusion.

Hence, to overcome these problems, we consider the advective Cahn–Hilliard (CH) equation. Let ϕ be the phase variable (i.e., $\phi = (m_1 - m_2)/(m_1 + m_2)$ where m_1 and m_2 are the masses of phases 1 and 2), then

$$\phi_t + \nabla \cdot (\phi \mathbf{u}) = M \Delta \mu,$$
$$\mu = F'(\phi) - \epsilon^2 \Delta \phi,$$

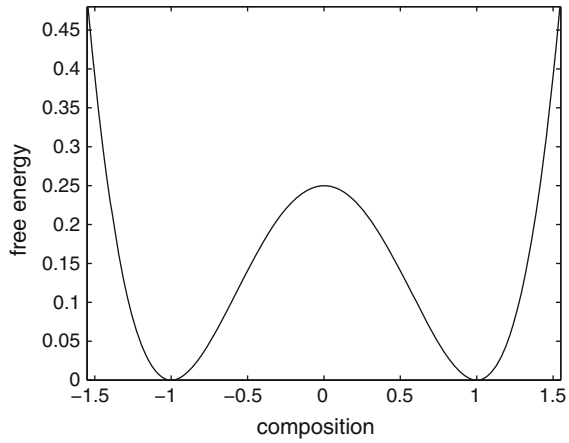

Fig. 3 Double well potential, $F(c) = 0.25(c^2 - 1)^2$

where M is the mobility, μ is the chemical potential, $F(\phi) = 0.25(\phi^2 - 1)^2$ is the Helmholtz free energy (see Fig. 3), and $\epsilon > 0$ is the interface thickness parameter. Ding et al. [35] derived the advective CH equation from the conservation law of mass of binary mixtures for fluids.

Therefore, the fluids are governed by the Navier–Stokes–Cahn–Hilliard (NSCH) equations [3,8,9,13,35,38,47–50,53–56]:

$$\rho(\phi)(\mathbf{u}_t + \mathbf{u} \cdot \nabla \mathbf{u}) = -\nabla p + \eta \Delta \mathbf{u} + \rho(\phi)\mathbf{g}, \tag{1}$$

$$\nabla \cdot \mathbf{u} = 0, \tag{2}$$

$$\phi_t + \nabla \cdot (\phi \mathbf{u}) = M \Delta \mu, \tag{3}$$

$$\mu = \phi^3 - \phi - \epsilon^2 \Delta \phi, \tag{4}$$

where $\rho(\phi) = \rho_1(1 + \phi)/2 + \rho_2(1 - \phi)/2$ is the variable density, η is the constant viscosity, and $\mathbf{g} = (0, -g)$. These are approximations to the complete Navier–Stokes equations. In this article, the effect of surface tension is neglected. We note that even though a phase-field method can deal with the variable viscosity case straightforwardly, we focus on viscosity-matched fluids since our main interest is the density variation.

In the Boussinesq approximation, the background density can be treated as a constant ρ_*, i.e., the variation of background density is neglected, and the difference between the actual density and ρ_* will contribute only to the buoyancy force term of the momentum equation [2]. Hence, Eq. 1 becomes

$$\rho_*(\mathbf{u}_t + \mathbf{u} \cdot \nabla \mathbf{u}) = -\nabla p + \eta \Delta \mathbf{u} + \rho(\phi)\mathbf{g}, \tag{5}$$

where $\rho_* = (\rho_1 + \rho_2)/2$ is the mean density [3,13]. The advantage of this model is that we solve a constant instead of a variable coefficient Poisson equation.

3 Review of the Boussinesq model

In this section, we briefly review previous studies using the Boussinesq approximation. Aref and Tryggvason [5] proposed a model for the development of the Rayleigh–Taylor instability in the Boussinesq approximation using concentrations of vorticity along the interface. In their case, the density was not coupled to a scalar field, and the buoyancy term in the Boussinesq Navier–Stokes equations was the only term related to the weak stratification. Han and Tryggvason [6] examined the deformation and breakup of axisymmetric drops, accelerated by a constant body force, for small density differences between the drops and the surrounding fluid. In their work, the density ratio was $\rho_1/\rho_2 = 1.15$ and a front tracking numerical technique was used to solve the unsteady Navier–Stokes equations for both the drops and the surrounding fluid. They showed, in the Boussinesq limit, as the Eötvös number increases

the drops break up in a backward facing bag, a transient breakup, and a forward facing bag mode. Young et al. [7] investigated the miscible Rayleigh–Taylor instability in both two and three dimensions. In their work, the fluid was assumed incompressible under the Boussinesq approximation to make the problem more tractable. They found that the 3D mixing zone expands two times faster than the 2D mixing zone through the simulation of randomly perturbed interfaces and identified three phases of evolution for the 3D mixing zone: the free-falling phase, the mixing phase, and the another free-falling phase. Liu and Shen [8] modeled the mixture of two incompressible fluids with a phase field model. A semi-discrete Fourier-spectral method for the numerical approximation of a Navier–Stokes system coupled with a CH equation was proposed and analyzed. They used the Boussinesq approximation to model the case where the two fluids have different densities.

Vladimirova and Rosner studied the fully nonlinear behavior of premixed flames in a gravitationally stratified medium, subject to the Boussinesq approximation in [10,11]. Vladimirova [12] simulated a bubble of reaction products rising in the reactant fluid under the influence of gravity using the Boussinesq buoyancy approximation. The Atwood numbers in their experiments were in the range of 0.075–0.16. The author showed that the evolution of the bubble can be divided into two stages: the bubble grows radially in an essentially motionless fluid in the first stage, and the bubble rises and is distorted by the flow during the second stage. Celani et al. [13] studied the Rayleigh–Taylor instability of two immiscible fluids in the limit of small Atwood numbers by means of a phase-field description. They analytically re-derived the known gravity–capillary dispersion relation in the limit of vanishing mixing energy density and capillary width, and numerical results were compared with known analytic results, both for the linearly stable and unstable cases, and for the weakly nonlinear stages of the latter. Forbes [14] studied the development of the Rayleigh–Taylor instability for inviscid and viscous fluids. The author used the approximate Boussinesq approach rather than the full Navier–Stokes equations of viscous flow and the density ratio was $\rho_1/\rho_2 = 1.05$. A separate spectral method was presented to study the Rayleigh–Taylor instability in a viscous Boussinesq fluid. The results were shown to agree closely with the inviscid calculations for small to moderate times. In [16], Boffetta et al. investigated the Rayleigh–Taylor turbulence in three dimensions at small Atwood number and at Prandtl number one by means of high resolution direct numerical simulations of the Boussinesq equations. The authors extended the mean-field analysis for velocity and temperature fluctuations and showed that small-scale velocity and temperature fluctuations develop intermittent distributions with structure function scaling exponents consistent with Navier–Stokes turbulence advecting a passive scalar.

4 The Boussinesq approximation model

If we add and subtract the term $\rho_* \mathbf{g}$ to and from Eq. 5, we get

$$\rho_*(\mathbf{u}_t + \mathbf{u} \cdot \nabla \mathbf{u}) = -\nabla p + \rho_* \mathbf{g} + \eta \Delta \mathbf{u} + (\rho(\phi) - \rho_*)\mathbf{g}. \tag{6}$$

In the 2D case, we can write Eq. 6 as follows:

$$\rho_*(\mathbf{u}_t + \mathbf{u} \cdot \nabla \mathbf{u}) = -\nabla(p + \rho_* g y) + \eta \Delta \mathbf{u} + (\rho(\phi) - \rho_*)\mathbf{g}. \tag{7}$$

If we reset the pressure field as $p = p + \rho_* g y$ and divide by ρ_*, then Eq. 7 becomes

$$\mathbf{u}_t + \mathbf{u} \cdot \nabla \mathbf{u} = -\frac{1}{\rho_*}\nabla p + \frac{\eta}{\rho_*}\Delta \mathbf{u} + \frac{\rho(\phi) - \rho_*}{\rho_*}\mathbf{g}.$$

The buoyancy contribution can be rewritten in terms of ρ_1, ρ_2, and ϕ as

$$\frac{\rho(\phi) - \rho_*}{\rho_*}\mathbf{g} = \frac{\rho_1(\frac{1+\phi}{2}) + \rho_2(\frac{1-\phi}{2}) - \rho_*}{\rho_*}\mathbf{g} = At\phi\mathbf{g}.$$

On the other hand, applying the similar procedure to the case of the variable density model, the buoyancy contribution in Eq. 1 can be rewritten as

$$\frac{\rho(\phi) - \rho_*}{\rho(\phi)}\mathbf{g} = \frac{At\phi}{1 + At\phi}\mathbf{g}.$$

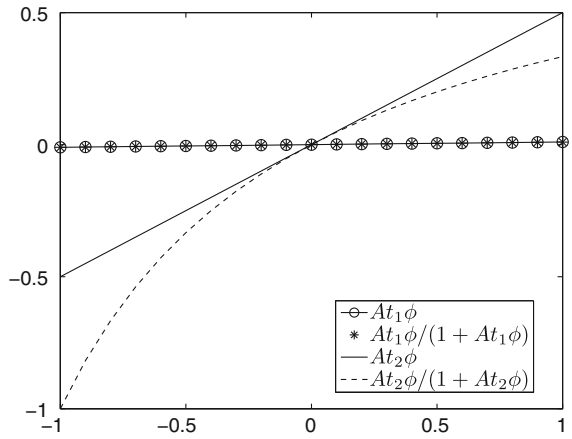

Fig. 4 Profiles of $At\phi$ (the Boussinesq case) and $At\phi/(1+At\phi)$ (the variable density case) for two different Atwood numbers $At_1 = 0.01$ and $At_2 = 0.5$

In our phase-field model, ϕ varies from -1 to 1. Note that $At\phi$ (the Boussinesq case) and $At\phi/(1+At\phi)$ (the variable density case) are linear and nonlinear functions with respect to the phase-field ϕ. Figure 4 shows profiles of $At\phi$ and $At\phi/(1+At\phi)$ for two different Atwood numbers $At = 0.01$ and $At = 0.5$. For $At = 0.01$, there is almost no difference between $At\phi$ and $At\phi/(1+At\phi)$, and both $At\phi$ and $At\phi/(1+At\phi)$ are nearly zero. However, for $At = 0.5$, there is a difference between $At\phi$ and $At\phi/(1+At\phi)$. This difference implies the difference of the buoyancy force. Figure 5a and b shows the buoyancy force for the Boussinesq and the variable density models with $At = 0.5$, respectively. In the case of the Boussinesq model, the buoyancy force is symmetric along the interface. However, in the case of the variable density model, the buoyancy force is not symmetric along the interface although the phase-field is symmetric. This difference of the buoyancy force causes a difference of the interface evolution for the Boussinesq and the variable density models. If the density variation goes to zero, i.e., $At \to 0$, then the difference between the Boussinesq and the non-Boussinesq fluids disappears. However, in general there is a difference between the Boussinesq and the non-Boussinesq fluids. Solutions of the two different models will be compared in the next section.

5 Numerical results

In this section, we compared the effect of the Boussinesq and the variable density models for the Rayleigh–Taylor instability with a phase-field method.

5.1 Relation between the Atwood number and the height of bubbles and spikes

In the Rayleigh–Taylor instability, fingers of the lighter fluid penetrate the heavier fluid as "bubbles," while "spikes" of the heavier fluid move into the lighter fluid. To investigate the relation between the Atwood number and the height of bubbles and spikes, we take an initial state as

$$\phi(x, y, 0) = \tanh\left(\frac{y - 2 - 0.1\cos(2\pi x)}{\sqrt{2}\epsilon}\right)$$

on the computational domain $\Omega = (0, 1) \times (0, 4)$. We perform simulations with a mesh size 128×512 and $\eta = 0.01$, $g = 10$, $M = 0.1$, $\Delta t = 2.0 \times 10^{-4}$, and $\epsilon = 0.01$. The zero level set of the initial profile is symmetric (see Fig. 6a). We define the height of bubbles (b_h) and spikes (s_h) as distance between two tangent lines (denoted by solid and dashed lines) of tips of bubbles and spikes, respectively (see Fig. 6b).

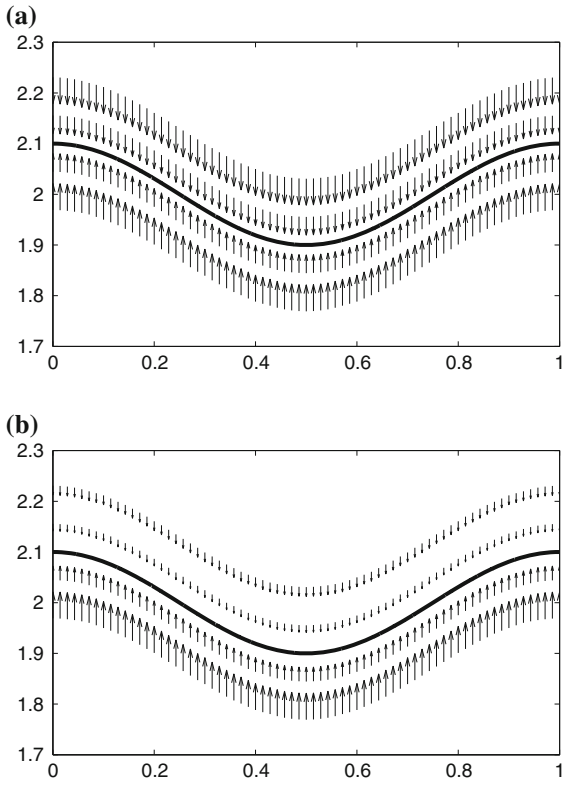

Fig. 5 The buoyancy force for **a** the Boussinesq approximation and **b** the variable density models with $At = 0.5$. This difference causes a difference of the interface evolution for the two different models

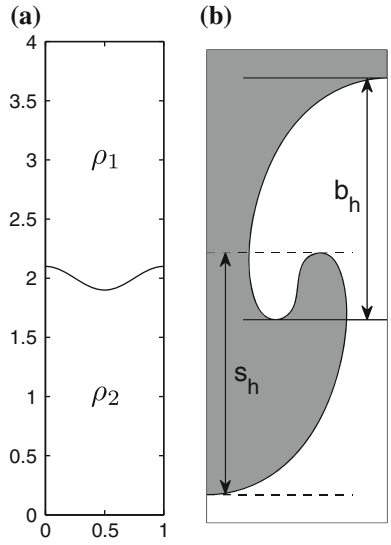

Fig. 6 **a** The zero level set of the initial profile, $\phi(x, y, 0) = \tanh\left(\frac{y-2-0.1\cos(2\pi x)}{\sqrt{2}\epsilon}\right)$. **b** Schematic for the measurement of the height of bubbles (b_h) and spikes (s_h)

Time evolution of the interface from the Boussinesq simulation with $At = 0.5$ is shown in Fig. 7. The times are shown below each figure. The symmetry of the heavy and light fronts for the Boussinesq flows can be clearly seen for a long time. Note that the symmetry can always be observed regardless of the Atwood number when we use the Boussinesq model. For the variable density models, Fig. 8a, b, and c shows concentration fields with $At = 0.1$ and $t = 2.32$, $At = 0.3$ and $t = 1.38$, and $At = 0.5$ and $t = 1.116$, respectively. Figure 8a still resembles the Boussinesq flows. Figure 8b shows that the heavy front moves faster than the light front. This observation can be seen even more clearly in Fig. 8c. As can be seen in Fig. 8, for the variable density flows, the symmetry is lost although the flow starts symmetrically. The phase shifts of the Boussinesq and the variable density flows with $At = 0.5$ are shown in Fig. 9. In Fig. 9, the circles are obtained by the symmetry about $y = 2$ and then a 90° phase shift of the symmetry-imposed phase. In the case of the Boussinesq model (Fig. 9a), the shifted phase is equivalent to the original phase, but it is not for the variable density model (Fig. 9b). The symmetry and non-symmetry of the heavy and light fronts affect heights of bubbles and spikes. Figure 10a shows the height of bubbles (b_h) versus height of spikes (s_h) with $At = 0.01, 0.1, 0.3$, and 0.5 for the Boussinesq and the variable density models. In the case of the Boussinesq model, the symmetry of the heavy and light fronts results in identical propagation heights of bubbles and spikes regardless of the value of the Atwood number. In the case of the variable density model, the height of spikes is almost the same as the height of bubbles when the Atwood number is very small. However, as the Atwood number increases, the height of spikes decreases compared with the height of bubbles. In Fig. 10b, the solid and dashed lines represent the interface of the Boussinesq ($t = 1.116$) and the variable density ($t = 1.116$) models for $At = 0.5$, respectively. In both cases, s_h is 1.2, and b_h of the Boussinesq and the variable density models are 1.2 and 1.45, respectively.

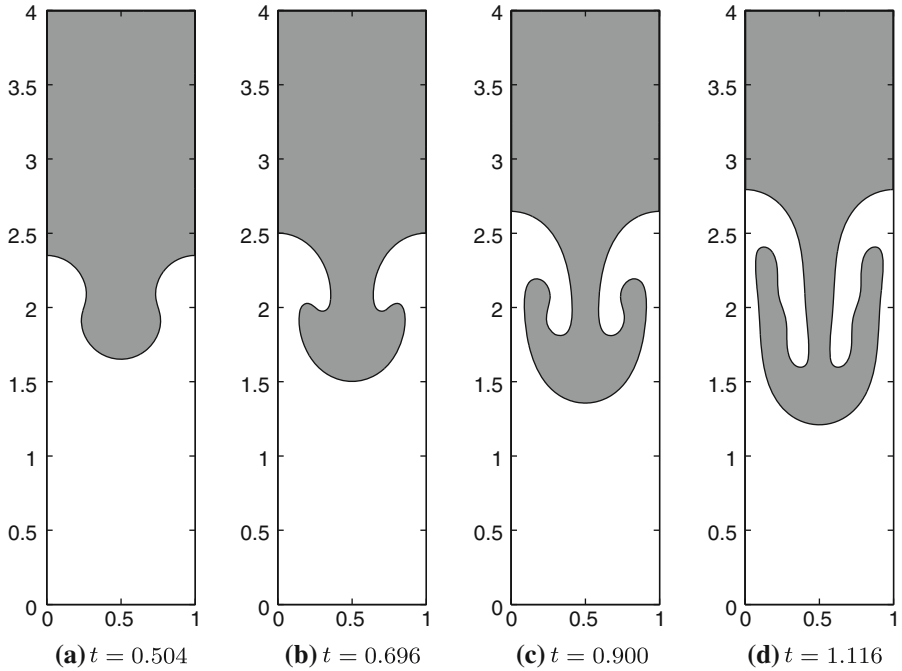

Fig. 7 Time evolution of the interface from the Boussinesq simulation with $At = 0.5$. The times are shown below each figure

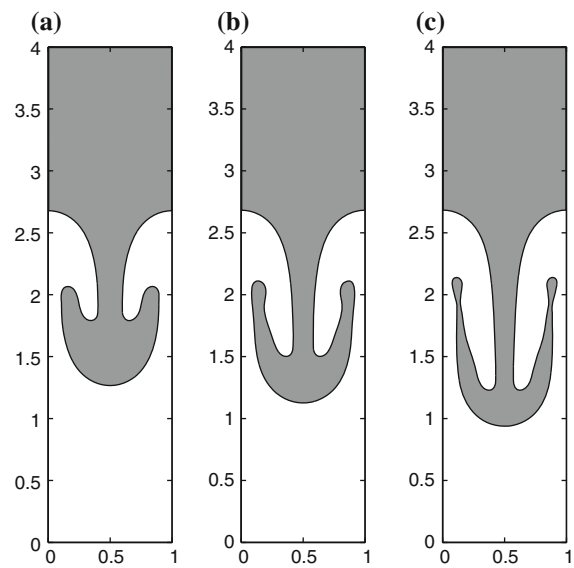

Fig. 8 Concentration fields from the non-Boussinesq simulation: **a** $At = 0.1$ and $t = 2.320$, **b** $At = 0.3$ and $t = 1.380$, and **c** $At = 0.5$ and $t = 1.116$

6 Conclusion

When density variations are sufficiently small the Boussinesq approximation is valid. The approximation is introduced to reduce the degree of the complexity of density variations and implies that density effects are considered only in the buoyancy force term of the momentum equation. Because of its simplicity in practical implementations, the approximation is widely used. Although there are many studies related to the approximation, some important characteristics are still missing. In this article, we compared the Boussinesq approximation and the variable density models for the 2D Rayleigh–Taylor instability with a phase-field method. Numerical experiments indicated that for

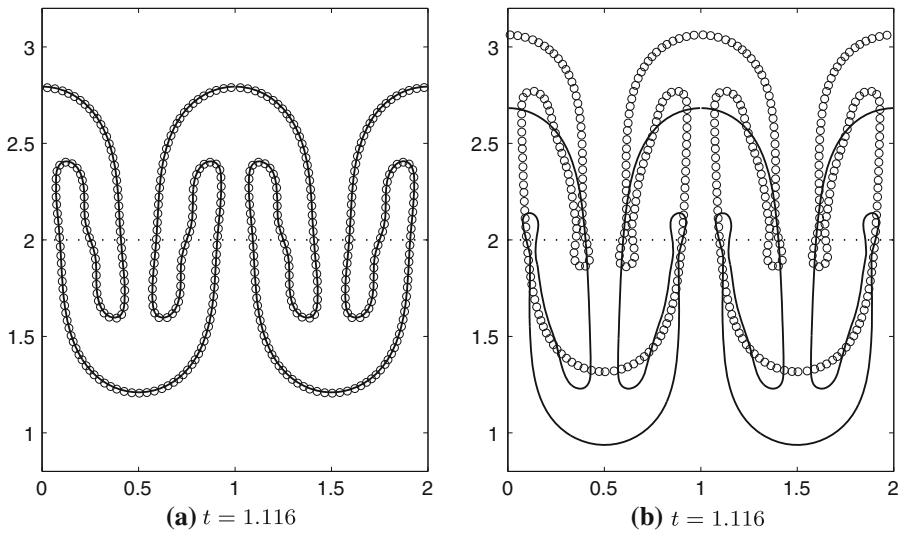

Fig. 9 The phase shifts for **a** the Boussinesq and **b** the variable density models with $At = 0.5$. The times are shown below each figure

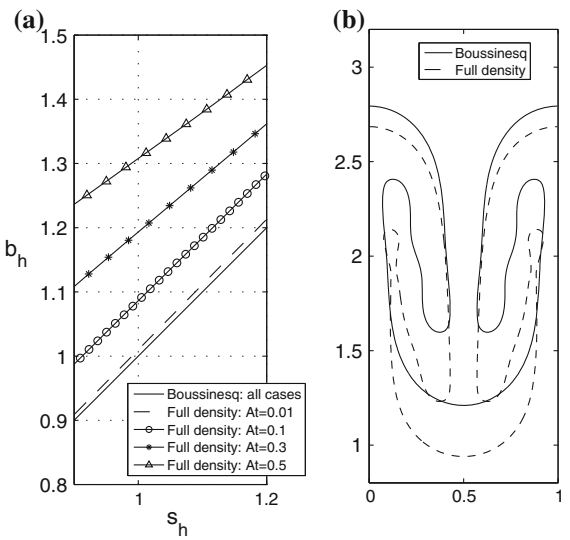

Fig. 10 **a** The height of bubbles (b_h) versus height of spikes (s_h) for $At = 0.01, 0.1, 0.3$, and 0.5. **b** The interface of the Boussinesq ($t = 1.116$) and the variable density ($t = 1.116$) models for $At = 0.5$. In both cases, s_h is 1.2, and b_h of the Boussinesq and the variable density models are 1.2 and 1.45, respectively

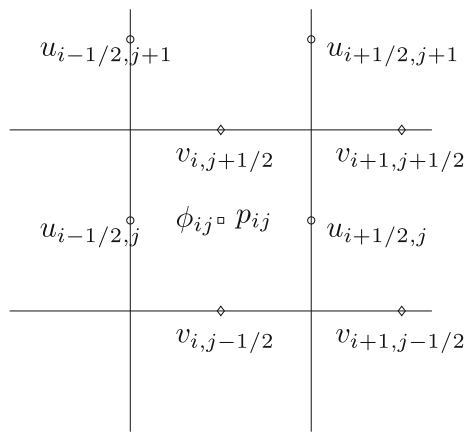

Fig. 11 Velocities are defined at cell boundaries while pressure and phase-fields are defined at the cell centers

an initially symmetric perturbation of the interface the symmetry of the heavy and light fronts for the Boussinesq model can be seen for a long time. However, for the variable density model the symmetry is lost although the flow starts symmetrically.

Acknowledgments This study was supported by the National Research Foundation of Korea (NRF) grant funded by the Korea government(MEST) (No. 2010-0027656). The authors thank anonymous referees for their respective helpful comments and suggestions.

Appendix A: Numerical solution

An efficient approximation can be obtained by decoupling the solution of the momentum equations from the solution of the continuity equation by a projection method [57–59]. The extension to three-dimensions is straightforward. We will focus on describing the idea in two-dimensions. In this section, we present the numerical solution for the Boussinesq approximation model. For the numerical solution of the variable density model, please refer to Ref. [38].

A staggered marker-and-cell (MAC) mesh of Harlow and Welch [60] is used in which pressure and phase-fields are stored at cell centers and velocities at cell boundaries (see Fig. 11).

Let a computational domain be partitioned in Cartesian geometry into a uniform mesh with mesh spacing h. The center of each cell, Ω_{ij}, is located at $(x_i, y_j) = ((i-0.5)h, (j-0.5)h)$ for $i = 1, \ldots, N_x$ and $j = 1, \ldots, N_y$. N_x and N_y are the numbers of cells in x and y-directions, respectively. The cell vertices are located at $(x_{i+\frac{1}{2}}, y_{j+\frac{1}{2}}) = (ih, jh)$. We denote by ∇_d, $\nabla_d \cdot$, and Δ_d the discrete gradient, divergence, and Laplacian, respectively. These are described in Eqs. 10 and 14.

At the beginning of each time step, given $\mathbf{u}^n$ and ϕ^n, we want to find $\mathbf{u}^{n+1}$, ϕ^{n+1}, and p^{n+1} which solve the following temporal discretization of Eqs. 2–4 and 7 of motion:

$$\rho_* \frac{\mathbf{u}^{n+1} - \mathbf{u}^n}{\Delta t} = -\rho_* (\mathbf{u} \cdot \nabla_d \mathbf{u})^n - \nabla_d p^{n+1} + \eta \Delta_d \mathbf{u}^n + (\rho^n - \rho_*)\mathbf{g},$$

$$\nabla_d \cdot \mathbf{u}^{n+1} = 0,$$

$$\frac{\phi^{n+1} - \phi^n}{\Delta t} = M \Delta_d \nu^{n+1} - M \Delta_d \phi^n - \nabla_d \cdot (\phi \mathbf{u})^n, \tag{8}$$

$$\nu^{n+1} = (\phi^{n+1})^3 - \epsilon^2 \Delta_d \phi^{n+1}, \tag{9}$$

where $\rho^n = \rho(\phi^n)$. The outline of the main procedures in one time step is:

Step 1. Initialize $\mathbf{u}^0$ to be the divergence-free velocity field and ϕ^0.

Step 2. Solve an intermediate velocity field, $\tilde{\mathbf{u}}$, which generally does not satisfy the incompressible condition, without the pressure gradient term,

$$\frac{\tilde{\mathbf{u}} - \mathbf{u}^n}{\Delta t} = -\mathbf{u}^n \cdot \nabla_d \mathbf{u}^n + \frac{\eta}{\rho_*} \Delta_d \mathbf{u}^n + \frac{\rho^n - \rho_*}{\rho_*} \mathbf{g}.$$

The resulting finite difference equations are written out explicitly. They take the form:

$$\begin{aligned} \tilde{u}_{i+\frac{1}{2},j} &= u^n_{i+\frac{1}{2},j} - \Delta t (u u_x + v u_y)^n_{i+\frac{1}{2},j} \\ &\quad + \frac{\Delta t \eta}{h^2 \rho_*} \left(u^n_{i+\frac{3}{2},j} + u^n_{i-\frac{1}{2},j} - 4u^n_{i+\frac{1}{2},j} + u^n_{i+\frac{1}{2},j+1} + u^n_{i+\frac{1}{2},j-1} \right), \end{aligned} \tag{10}$$

$$\begin{aligned} \tilde{v}_{i,j+\frac{1}{2}} &= v^n_{i,j+\frac{1}{2}} - \Delta t (u v_x + v v_y)^n_{i,j+\frac{1}{2}} - \frac{\Delta t \left(\rho^n_{i,j+\frac{1}{2}} - \rho_* \right) g}{\rho_*} \\ &\quad + \frac{\Delta t \eta}{h^2 \rho_*} \left(v^n_{i+1,j+\frac{1}{2}} + v^n_{i-1,j+\frac{1}{2}} - 4v^n_{i,j+\frac{1}{2}} + v^n_{i,j+\frac{3}{2}} + v^n_{i,j-\frac{1}{2}} \right). \end{aligned}$$

Details for the calculation of the advection terms are presented in [38].

Then, we solve the following equations for the advanced pressure field at $(n+1)$ time step:

$$\frac{\mathbf{u}^{n+1} - \tilde{\mathbf{u}}}{\Delta t} = -\frac{1}{\rho_*} \nabla_d p^{n+1}, \tag{11}$$

$$\nabla_d \cdot \mathbf{u}^{n+1} = 0. \tag{12}$$

With application of the divergence operator to Eq. 11, we find the Poisson equation for the pressure at the advanced time $(n+1)$.

$$\frac{1}{\rho_*} \Delta_d p^{n+1} = \frac{1}{\Delta t} \nabla_d \cdot \tilde{\mathbf{u}}, \tag{13}$$

where we have made use of Eq. 12 and the terms are defined as in the following:

$$\Delta_d p_{ij}^{n+1} = \frac{p_{i+1,j}^{n+1} + p_{i-1,j}^{n+1} - 4p_{ij}^{n+1} + p_{i,j+1}^{n+1} + p_{i,j-1}^{n+1}}{h^2},$$
$$\nabla_d \cdot \tilde{\mathbf{u}}_{ij} = \frac{\tilde{u}_{i+\frac{1}{2},j} - \tilde{u}_{i-\frac{1}{2},j}}{h} + \frac{\tilde{v}_{i,j+\frac{1}{2}} - \tilde{v}_{i,j-\frac{1}{2}}}{h}. \tag{14}$$

The boundary condition for the pressure is

$$\mathbf{n} \cdot \nabla_d p^{n+1} = \mathbf{n} \cdot \left(-\rho_* \frac{\mathbf{u}^{n+1} - \mathbf{u}^n}{\Delta t} - \rho_* (\mathbf{u} \cdot \nabla_d \mathbf{u})^n + \eta \Delta_d \mathbf{u}^n + (\rho^n - \rho_*)\mathbf{g} \right),$$

where $\mathbf{n}$ is the unit normal vector to the domain boundary.

In our application of the phase-field to the Rayleigh–Taylor instability, we will use a periodic boundary condition to vertical boundaries and no slip boundary condition to the top and bottom domains. Therefore,

$$\mathbf{n} \cdot \nabla_d p^{n+1} = \mathbf{n} \cdot (\rho^n - \rho_*)\mathbf{g}, \text{ i.e., } \frac{\partial p}{\partial y} = -(\rho^n - \rho_*)g \text{ at } y = 0 \text{ and } y = L_y.$$

The resulting linear system of Eq. 13 is solved using a multigrid method [61], specifically, V-cycles with a Gauss–Seidel relaxation. Then the divergence-free normal velocities u^{n+1} and v^{n+1} are defined by

$$\mathbf{u}^{n+1} = \tilde{\mathbf{u}} - \frac{\Delta t}{\rho_*} \nabla_d p^{n+1},$$
$$\text{i.e., } u_{i+\frac{1}{2},j}^{n+1} = \tilde{u}_{i+\frac{1}{2},j} - \frac{\Delta t}{\rho_* h}(p_{i+1,j} - p_{ij}), \quad v_{i,j+\frac{1}{2}}^{n+1} = \tilde{v}_{i,j+\frac{1}{2}} - \frac{\Delta t}{\rho_* h}(p_{i,j+1} - p_{ij}).$$

We implement the unconditionally gradient stable scheme in Eqs. 8 and 9 with a nonlinear multigrid method. For a detailed description of the numerical method used in solving these equations, please refer to Refs. [62,63].

In our simulations, mass conservation is an important factor. Therefore, we use a conservative discretization of the convective part of the phase-field equation (8).

$$((\phi u)_x + (\phi v)_y)_{ij}^n = \frac{u_{i+\frac{1}{2},j}^n (\phi_{i+1,j}^n + \phi_{ij}^n) - u_{i-\frac{1}{2},j}^n (\phi_{ij}^n + \phi_{i-1,j}^n)}{2h} + \frac{v_{i,j+\frac{1}{2}}^n (\phi_{i,j+1}^n + \phi_{ij}^n) - u_{i,j-\frac{1}{2}}^n (\phi_{ij}^n + \phi_{i,j-1}^n)}{2h}.$$

These complete one time step.

References

1. Boussinesq J (1903) Theorie analytique de la chaleur, vol 2. Gauthier-Villars, Paris
2. Lighthill J (1978) Waves in fluids. Cambridge University Press, Cambridge
3. Jacqmin D (1999) Calculation of two-phase Navier–Stokes flows using phase-field modeling. J Comput Phys 155:96–127
4. Tryggvason G (1988) Numerical simulations of the Rayleigh–Taylor instability. J Comput Phys 75:253–282
5. Aref H, Tryggvason G (1989) Model of Rayleigh–Taylor instability. Phys Rev Lett 62:749–752
6. Han J, Tryggvason G (1999) Secondary breakup of axisymmetric liquid drops. I. Acceleration by a constant body force. Phys Fluids 11:3650–3667
7. Young Y-N, Tufo H, Dubey A, Rosner R (2001) On the miscible Rayleigh–Taylor instability: two and three dimensions. J Fluid Mech 447:377–408
8. Liu C, Shen J (2003) A phase field model for the mixture of two incompressible fluids and its approximation by a Fourier-spectral method. Physica D 179:211–228
9. Kim JS, Lowengrub JS (2005) Phase field modeling and simulation of three-phase flows. Interface Free Bound 7:435–466
10. Vladimirova N, Rosner R (2003) Model flames in the Boussinesq limit: the effects of feedback. Phys Rev E 67:066305-1–066305-10
11. Vladimirova N, Rosner R (2005) Model flames in the Boussinesq limit: the case of pulsating fronts. Phys Rev E 71:067303-1–067303-4
12. Vladimirova N (2007) Model flames in the Boussinesq limit: rising bubbles. Combust Theor Model 11:377–400
13. Celani A, Mazzino A, Muratore-Ginanneschi P, Vozella L (2009) Phase-field model for the Rayleigh–Taylor instability of immiscible fluids. J Fluid Mech 622:115–134
14. Forbes LK (2009) The Rayleigh–Taylor instability for inviscid and viscous fluids. J Eng Math 65:273–290

15. Forbes LK (2011) A cylindrical Rayleigh–Taylor instability: radial outflow from pipes or stars. J Eng Math 70:205–224
16. Boffetta G, Mazzino A, Musacchio S, Vozella L (2010) Statistics of mixing in three-dimensional Rayleigh–Taylor turbulence at low Atwood number and Prandtl number one. Phys Fluids 22:035109-1–035109-8
17. Unverdi SO, Tryggvason G (1992) A front-tracking method for viscous, incompressible, multi-fluid flows. J Comput Phys 100: 25–37
18. Popinet S, Zaleski S (1999) A front-tracking algorithm for accurate representation of surface tension. Int J Numer Methods Fluids 30:775–793
19. Glimm J, Grove JW, Li XL, Oh W, Sharp DH (2001) A critical analysis of Rayleigh–Taylor growth rates. J Comput Phys 169: 652–677
20. Liu X, Li Y, Glimm J, Li XL (2007) A front tracking algorithm for limited mass diffusion. J Comput Phys 222:644–653
21. Terashima H, Tryggvason G (2009) A front-tracking/ghost-fluid method for fluid interfaces in compressible flows. J Comput Phys 228:4012–4037
22. Hirt CW, Nichols BD (1981) Volume of fluid (VOF) method for the dynamics of free boundaries. J Comput Phys 39:201–225
23. Rudman M (1997) Volume-tracking methods for interfacial flow calculations. Int J Numer Methods Fluids 24:671–691
24. Gerlach D, Tomar G, Biswas G, Durst F (2006) Comparison of volume-of-fluid methods for surface-tension dominant two-phase flows. Int J Heat Mass Transf 49:740–754
25. Gopala VR, Wachem BGMvan (2008) Volume of fluid methods for immiscible-fluid and free-surface flows. Chem Eng J 141: 204–221
26. Raessi M, Mostaghimi J, Bussmann M (2010) A volume-of-fluid interfacial flow solver with advected normals. Comput Fluids 39:1401–1410
27. Nie X, Qian Y-H, Doolen GD, Chen S (1998) Lattice Boltzmann simulation of the two-dimensional Rayleigh–Taylor instability. Phys Rev E 58:6861–6864
28. He X, Chen S, Zhang R (1999) A lattice Boltzmann scheme for incompressible multiphase flow and its application in simulation of Rayleigh–Taylor instability. J Comput Phys 152:642–663
29. He X, Zhang R, Chen S, Doolen GD (1999) On the three-dimensional Rayleigh–Taylor instability. Phys Fluids 11:1143–1152
30. Clark TT (2003) A numerical study of the statistics of a two-dimensional Rayleigh–Taylor mixing layer. Phys Fluids 15:2413–2423
31. Chang YC, Hou TY, Merriman B, Osher S (1996) A level set formulation of Eulerian interface capturing methods for incompressible fluid flows. J Comput Phys 124:449–464
32. Gomez P, Hernandez J, Lopez J (2005) On the reinitialization procedure in a narrow-band locally refined level set method for interfacial flows. Int J Numer Methods Eng 63:1478–1512
33. Herrmann M (2008) A balanced force refined level set grid method for two-phase flows on unstructured flow solver grids. J Comput Phys 227:2674–2706
34. Sheu TWH, Yu CH, Chiu PH (2009) Development of a dispersively accurate conservative level set scheme for capturing interface in two-phase flows. J Comput Phys 228:661–686
35. Ding H, Spelt PDM, Shu C (2007) Diffuse interface model for incompressible two-phase flows with large density ratios. J Comput Phys 226:2078–2095
36. Sun Y, Beckermann C (2008) A two-phase diffuse-interface model for Hele–Shaw flows with large property contrasts. Physica D 237:3089–3098
37. Chiu P-H, Lin Y-T (2011) A conservative phase field method for solving incompressible two-phase flows. J Comput Phys 230: 185–204
38. Lee HG, Kim K, Kim J (2011) On the long time simulation of the Rayleigh–Taylor instability. Int J Numer Methods Eng 85: 1633–1647
39. Rayleigh L (1883) Investigation of the character of the equilibrium of an incompressible heavy fluid of variable density. Proc Lond Math Soc 14:170–177
40. Taylor G (1950) The instability of liquid surfaces when accelerated in a direction perpendicular to their planes. I Proc R Soc Lond A 201:192–196
41. Atzeni S, Meyer-Ter-Vehn J (2004) The physics of inertial fusion: beam plasma interaction, hydrodynamics, hot dense matter. Oxford University Press, Oxford, USA
42. Buchler JR, Livio M, Colgate SA (1980) Supernova explosions—the role of a Rayleigh–Taylor instability. Space Sci Rev 27: 571–577
43. Brecht SH, Papadopoulos K (2002) Cross field jetting of energetic ions produced by Rayleigh–Taylor instability. Naval Research Laboratory, Washington
44. Debnath L (1994) Nonlinear water waves. Academic Press, Boston
45. Keskinen MJ, Ossakow SL, Szuszczewicz EP, Holmes JC (1981) Nonlinear theory and experimental observations of the local collisional Rayleigh–Taylor instability in a descending equatorial spread F ionosphere. J Geophys Res 86:5785–5792
46. Ribeyre X, Tikhonchuk VT, Bouquet S (2004) Compressible Rayleigh–Taylor instabilities in supernova remnants. Phys Fluids 16:4661–4670
47. Badalassi VE, Ceniceros HD, Banerjee S (2003) Computation of multiphase systems with phase field models. J Comput Phys 190:371–397
48. Yue P, Feng JJ, Liu C, Shen J (2004) A diffuse-interface method for simulating two-phase flows of complex fluids. J Fluid Mech 515:293–317

49. Kim C-H, Shin S-H, Lee HG, Kim J (2009) Phase-field model for the pinchoff of liquid-liquid jets. J Korean Phys Soc 55:1451–1460
50. Kim J (2009) A generalized continuous surface tension force formulation for phase-field models for multi-component immiscible fluid flows. Comput Methods Appl Mech Eng 198:3105–3112
51. Biben T, Kassner K, Misbah C (2005) Phase-field approach to three-dimensional vesicle dynamics. Phys Rev E 72:041921-1–041921-115
52. Ferziger JH, Peric M (2002) Computational methods for fluid dynamics. Springer, Berlin
53. Chella R, Viñals J (1996) Mixing of a two-phase fluid by cavity flow. Phys Rev E 53:3832–3840
54. Jacqmin D (2000) Contact-line dynamics of a diffuse fluid interface. J Fluid Mech 402:57–88
55. Kim J (2005) A continuous surface tension force formulation for diffuse-interface models. J Comput Phys 204:784–804
56. Boyer F, Lapuerta C (2006) Study of a three component Cahn–Hilliard flow model. M2AN 40:653–687
57. Bell JB, Colella P, Glaz HM (1989) A second-order projection method for the incompressible Navier–Stokes equations. J Comput Phys 85:257–283
58. Chorin AJ (1967) A numerical method for solving incompressible viscous flow problems. J Comput Phys 2:12–26
59. Li J, Renardy Y (2000) Numerical study of flows of two immiscible liquids at low Reynolds number. SIAM Rev 42:417–439
60. Harlow FH, Welch JE (1965) Numerical calculation of time-dependent viscous incompressible flow of fluid with free surface. Phys Fluids 8:2182–2189
61. Trottenberg U, Oosterlee C, Schüller A (2001) Multigrid. Academic Press, New York, USA
62. Kim J (2007) A numerical method for the Cahn–Hilliard equation with a variable mobility. Commun Nonlinear Sci Numer Simul 12:1560–1571
63. Kim J, Bae H-O (2008) An unconditionally stable adaptive mesh refinement for Cahn–Hilliard equation. J Korean Phys Soc 53:672–679